Princeton Plasma Physics Laboratory

PPPL-

PPPL-

PRINCETON PLASMA PHYSICS LABORATORY

Princeton Plasma Physics Laboratory
Report Disclaimers

Full Legal Disclaimer

Trademark Disclaimer

PPPL Report Availability

Princeton Plasma Physics Laboratory:

http://www.pppl.gov/techreports.cfm

Office of Scientific and Technical Information (OSTI):

http://www.osti.gov/bridge

Related Links:

U.S. Department of Energy

Office of Scientific and Technical Information

Fusion Links

Experimental Evaluation of Multi-spacecraft Data Analysis Techniques in a Laboratory Plasma

Jongsoo Yoo and Masaaki Yamada

March 26, 2012

Abstract

The Magnetic Reconnection Experiment (MRX)[1] has been utilized to assess the effectiveness of minimum variance analysis on the magnetic field (MVAB) and boundary-crossing time analysis (BCTA). The neutral sheet is swept, or jogged, in a controlled manner with respect to the stationary probes by pulsed internal coil currents. Magnetic field data from measurement points resembling data from multi-spacecraft flying though a reconnecting current sheet is used to check both techniques to deduce a proper normal vector. We examine discharges with the two-dimensional (2-D) X-line structure as well as cases in which a flux rope forms within the layer. All discharges are in a two-fluid regime in which electrons are magnetized but not ions. Boundary-crossing time analysis with four sample measurement points forming a tetrahedron generates a reasonable unit normal vector and relative velocity along the normal vector for all of the tested cases. On the other hand, MVAB sometimes fails to predict a proper normal direction. This is because the X-line magnetic geometry is fundamentally 2-D or 3-D. However, the direction along the reconnecting field determined by MVAB does not deviate much from the real magnetic geometry documented by 2-D magnetic probe arrays and one additional probe at a different toroidal location. Based on these observations, we suggest a procedure for determining a local coordinate system for data from the Magnetospheric Multi-Scale (MMS) mission when spacecraft passes through a reconnecting current sheet. The distance between measurement points on the order of the ion skin depth (c/ω_{pi}) is pertinent to determination of the magnetic geometry.

1 Introduction

For many decades, satellite measurements have been employed to understand the complex nature of the magnetic fields surrounding the Earth. During the past dozen years in particular, the role of magnetic reconnection has been explored in detail through the combined effort of numerical simulations, dedicated laboratory plasma experiments, and direct observations from spacecraft [2]. Now it is recognized that two-fluid effects [3, 4], resulting from the different behavior of ions and electrons in the reconnection layer, play a key role in collisionless reconnection.

The Magnetospheric Multi-Scale (MMS) mission, which will be launched in 2014, is the first space mission able to explore down to spatial scales of the order of the electron inertial length (c/ω_{pe}), a measurement regime which is critical to a complete understanding of collisionless reconnection. During the mission, four spacecraft will be placed in a tetrahedron configuration at various distances as they pass through the Earth's magnetopause and magnetotail to make detailed measurements of reconnection. The Magnetic Reconnection Experiment (MRX) research program is primarily dedicated to the development of a fundamental understanding of magnetic reconnection layer physics through a dedicated laboratory experiment. Presently, we are undertaking a mini-campaign in MRX designed to provide feedback to the MMS mission, which may ultimately impact spacecraft separations, orbits, data collection strategies, and instrument capabilities before and after the MMS launch.

In particular, one of the biggest challenges associated with measurements of reconnection using spacecraft is the ability to identify the magnetic field geometry. Because the number of spacecraft is limited, the spatial

profile of the plasma has to be inferred from the time series of physical quantities, such as the magnetic field and electric field, typically using at most four locations. Several analysis methods have been developed to gain traction on this problem. Classical minimum variance analysis on magnetic field data (known as MVAB) [5] has been employed for many spacecraft data analyses [e.g. *Øieroset et al.*, 2001] [6]. Alternatively, maximum variance analysis of electric field data (MVAE) [7, 8], or the Faraday residue method [9, 10] can be employed if electric field measurements are also available. These variance analysis methods (MVAB, MVAE, and the Faraday residue method) can be used to identify a vector normal to the reconnection current layer using data from a single spacecraft. When four spacecraft encounter any kind of planar boundary, for example a 1-D shock front and a current sheet, a more accurate $\hat{\mathbf{n}}$ and V_n can be estimated via boundary-crossing time analysis [11].

For a study of reconnection, however, more information on the magnetic geometry is needed: knowing the direction normal to the current sheet is not enough. Key physical parameters such as the reconnection rate cannot be estimated without differentiating two tangential directions: the out-of-plane direction and the direction of the reconnecting electric field. When MVAB or MVAE successfully separates all three principal axes, they naturally form a coordinate system, so that the full local magnetic geometry can be inferred. However, when the variance along two principal axes are similar, they may not reconstruct the magnetic geometry properly. *Mozer and Retinò* [2007] combine MVAB and MVAE to find the rotation matrix transforming the GSE coordinate system into the magnetopause frame for study of 120 magnetopause crossings by noticing that MVAB best finds the direction of the reconnecting magnetic field component which is the maximum varying component, while MVAE best locates the maximum varying normal electric field component [12].

In this report, we present a detailed and elaborate laboratory test of two of the methods mentioned above, minimum variance analysis of the magnetic field (MVAB) and boundary-crossing time analysis, in a collisionless reconnection layer. Since MRX routinely makes global measurements of the magnetic field, the true geometry of the layer is known and the methods can be quantitatively checked. The main objective of this paper is to identify whether a proper magnetic geometry can be reproduced by MVAB and boundary-crossing time analysis by utilizing data from the Magnetic Reconnection Experiment (MRX). We do not perform MVAE or the Faraday residual analysis because we do not currently have sufficient electric field measurement capabilities.

In the present experimental campaign on MRX, the current sheet is swept over the stationary probes via internal pulsed coils. This situation is very similar to the space measurements in which the current sheet moves with respect to spacecraft. This plasma "jogging" experiment is carefully designed and performed so that we can test these methods in the plasma in which we monitor evolution of the entire profile of the magnetic field.

2   Experimental Apparatus

In MRX plasmas, the MHD criteria ($S \gg 1$, $\rho_i \ll L$, where S is the Lundquist number; ρ_i is the ion gyroradius; L is the system scale length) are satisfied in the bulk of the plasma [1]. Figure 1 shows a cross section of the MRX vacuum vessel for this experimental campaign in the $R - Z$ plane. The two gray circles indicate flux cores, each of which contains two independent sets of coils: a poloidal field (PF) coil and a toroidal field (TF) coil [13]. The PF coil generates the X-line geometry at the middle of the MRX device and drives magnetic reconnection, while the TF coil creates the plasma inductively around the flux cores. As the toroidal (out-of-plane) current of PF coils ramps down, the magnetic flux is pulled towards the flux cores and a current sheet elongated along the Z direction (indicated in orange in figure 1) is formed. In this phase, the initial out-of-plane magnetic field during the plasma formation becomes negligible compared to the reconnecting magnetic field, so that anti-parallel reconnection is achieved. The whole process of the plasma formation and magnetic reconnection are monitored by 2-D magnetic probe arrays located every 3 cm from $Z = -9$ cm to 9 cm and electrostatic probes such as Langmuir probes and Mach probes. The maximum radial resolution of the magnetic arrays is 0.6 cm and the radial coverage is 16 cm. Data is acquired every 0.4 μs.
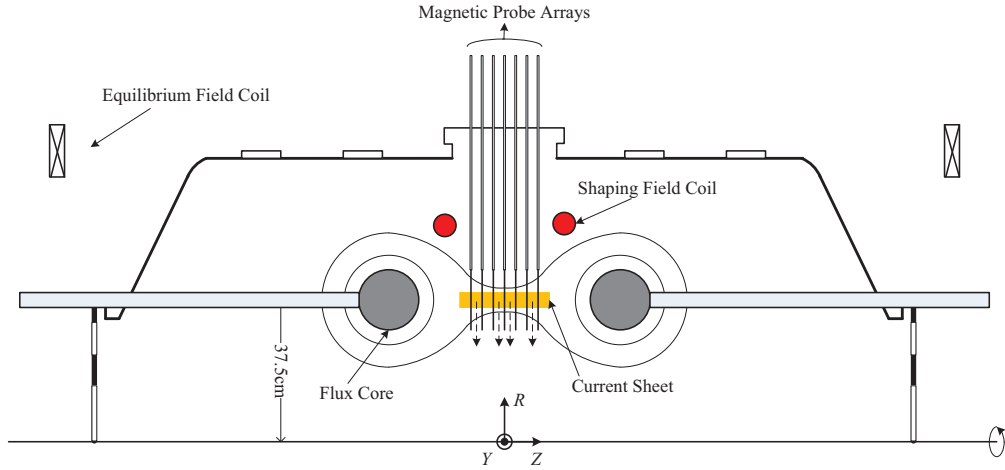
Figure 1: Cross section of the MRX vacuum chamber. The gray circles indicate flux cores in which there are two sets of coils: poloidal field (PF) coils and toroildal field (TF) coils. PF coils produce the X-line geometry and drive reconnection. The red circles show the position of the shaping field (SF) coils which are used to accelerate the motion of the current sheet radially inward.

Figure 2: Current sheet motion as a function of the firing voltage for the SF coils. Shortly after the SF coils are activated, the current sheet starts to move in. The jogging speed of the current sheet is proportional to the firing voltage. Two black dashed lines indicate the quasi-steady period of the MRX plasma.

3

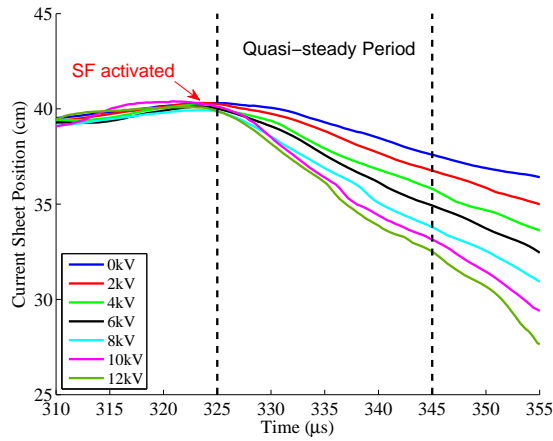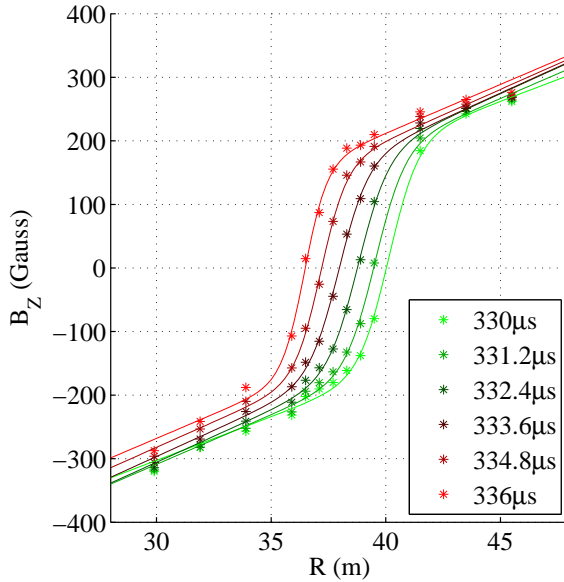Figure 3: Radial profiles of B_Z every 1.2 μs during the quasi-steady period of a single discharge, measured by the magnetic probe array at $Z = 0$. Asterisks stand for measured data and the solid lines come from fitting the data to a Harris function, $\sim \tanh((R - R_0)/\delta)$. The current sheet moves in with a relatively well-maintained structure at about 5.8 km/s.

In this experimental campaign, there is another set of coils (red circles in figure 1) called the shaping field (SF) coils by which the radially inward motion of the MRX current sheet is accelerated, or jogged. The advantage of this laboratory experiment is that a simulated "satellite" data set can be obtained when the current sheet region is swept past a stationary probe with a predetermined velocity and angle. The jogging speed of the current sheet can be controlled by firing the SF coils with various voltages. Figure 2 shows time profiles of the current sheet location with various SF firing voltages. The SF coils are activated just before the quasi-steady period of the MRX plasma. Shortly after they are fired, the current sheet moves in radially. The location is tracked by fitting radial B_Z profiles into a Harris-sheet type function [14], $\sim \tanh((R - R_0)/\delta)$ [?]. The moving-in speed increases almost linearly with the firing voltage. Figure 3 illustrates radial profiles of B_Z during the quasi-steady period of a single discharge. Asterisks stand for measured data and solid lines are from a Harris function fit. The current sheet moves in while maintaining its structure well. In this discharge, the current sheet moves about 3.5 cm over 6 μs, yielding a speed of 5.8 km/s, which is about one order of magnitude lower than the Alfvén velocity based on upstream plasma parameters ($n_e = 2 - 5 \times 10^{13}$ cm^{-3} and $|\mathbf{B}| = 200 - 250$ Gauss). Every discharge presented in this paper has a similar radial speed ($5 - 6$ km/s).

3   Minimum Variance Analysis on Magnetic Field

The following coordinate system which is similar to the GSE system for subsolar reconnection is used throughout this paper: x is normal to the current sheet, y is along the out-of-plane direction, and z is in the direction of the reconnecting magnetic field, following *Mozer and Retinó* [2007] [12]. The corresponding local Cartesian coordinates for reconnection during the quasi-steady period in MRX are R, Y, and Z respectively [1].

The theory behind MVAB can be found in the literature [5, 15]. The fundamental assumption is that

the boundary is one-dimensional: physical quantities vary only along the direction normal to the layer. For the magnetic field, this assumption means

$$\nabla \cdot \mathbf{B} = \frac{\partial B_n}{\partial n} = 0, \tag{1}$$

and

$$\frac{\partial B_n}{\partial t} = -(\nabla \times \mathbf{E})_n = 0. \tag{2}$$

In other words, the magnetic field component normal to the boundary does not vary while spacecraft passes by it. In reality, however, due to 2-D or 3-D structures and temporal variations, the normal component undergoes finite changes. The basic idea of MVAB is that the direction along which the magnetic field component varies least would be a good indicator of the normal vector $\hat{\mathbf{n}}$: for a given set of M magnetic field measurements spanning the boundary layer crossing time, we need to find $\hat{\mathbf{n}}$ that minimizes the variance

$$\sigma^2 = \frac{1}{M} \sum_{m=1}^{M} \left| \left(\mathbf{B}^{(m)} - \langle \mathbf{B} \rangle \right) \cdot \hat{\mathbf{n}} \right|^2, \tag{3}$$

where $\mathbf{B}^{(m)}$ is the m-th measured magnetic field record of the data and the average $\langle \mathbf{B} \rangle$ is just

$$\langle \mathbf{B} \rangle \equiv \frac{1}{M} \sum_{m=1}^{M} \mathbf{B}^{(m)}. \tag{4}$$

Such a unit vector $\hat{\mathbf{n}}$ can be found by computing eigenvectors of the symmetric matrix $\mathbf{M}$ defined by

$$M_{\mu\nu} = \langle B_\mu B_\nu \rangle - \langle B_\mu \rangle \langle B_\nu \rangle, \tag{5}$$

where B_μ and B_ν are components of the measured magnetic field based on a Cartesian coordinate system. For MRX data, they are B_R, B_Y, and B_Z. Since the magnetic variance matrix $\mathbf{M}$ is symmetric, three eigenvalues λ_1, λ_2, and λ_3 in the order of increasing magnitude are real and corresponding normalized eigenvectors $\mathbf{u}_1$, $\mathbf{u}_2$, and $\mathbf{u}_3$ are orthogonal. Mathematically, each eigenvalue equals the variance along the corresponding eigenvector. Thus, if a spacecraft encounters the current sheet and passes though it, the normalized eigenvector $\mathbf{u}_1$ that has the minimum variance is a natural choice for the unit normal vector $\hat{\mathbf{n}}$, or $\hat{\mathbf{x}}$. Because magnetic field component along the direction of the reconnecting magnetic field B_z varies most across the layer, $\mathbf{u}_2$ and $\mathbf{u}_3$ are parallel to $\mathbf{y}$ and $\mathbf{z}$ respectively.

The size of the data segment, M, is chosen by checking that the results of MVAB are stationary. If the basic assumption of MVAB is satisfied, i.e. if the boundary is 1-D, MVAB is independent of the number of data points. This stationary property of MVAB is not guaranteed in real data. If M is too small or too large, results from MVAB can be different from those with intermediate data segments [15]. Thus, the stationarity of MVAB must be checked to make sure the nested data segment is within the intermediate, or "plateau" region. The smallest data set for MVAB has three points - the center point which is closest to the boundary and one from each side. The next smallest data segment is constructed by adding one data point to each side. As M increases, the average magnetic field along the normal vector from MVAB $< \mathbf{B} > \cdot \hat{\mathbf{n}}$ remains nearly unchanged, indicating a plateau region as shown in figure 6-(a). The number of data points M is chosen such that the data segment is in the plateau region.

To summarize the procedure of determining local coordinates by MVAB, a proper span of magnetic field data centered at the middle of the current sheet must be chosen. Then, the magnetic variance matrix $\mathbf{M}$ is constructed with the data, and eigenvalues and eigenvectors of $\mathbf{M}$ are computed. The normalized eigenvector corresponding to the smallest eigenvalue determines the normal direction $\hat{\mathbf{x}}$, i.e., $\hat{\mathbf{x}} = \pm\mathbf{u}_1$. The other two eigenvectors $\mathbf{u}_2$ and $\mathbf{u}_3$ define $\hat{\mathbf{y}}$ and $\hat{\mathbf{z}}$. Proper signs should be chosen to make sure $\hat{\mathbf{z}} = \hat{\mathbf{x}} \times \hat{\mathbf{y}}$. Then, the transformation of values in the original cartesian coordinates (R, Y, Z) into those in (x, y, z) is given by

$$\begin{pmatrix} x \\ y \\ z \end{pmatrix} = \begin{pmatrix} \hat{\mathbf{x}} \\ \hat{\mathbf{y}} \\ \hat{\mathbf{z}} \end{pmatrix} \begin{pmatrix} R \\ Y \\ Z \end{pmatrix}. \tag{6}$$

4   MVAB for MRX Jogging Experiment

Data from the MRX jogging experiment provides a good opportunity to test MVAB since the full 2-D (or 3-D) magnetic field geometry is measured. Whether MVAB generates a proper normal vector can be easily checked by comparing the local magnetic geometry predicted by MVAB with the measured global geometry.

Figure 4 shows the time evolution of 2-D profiles of the current density J_Y with contours of the poloidal magnetic flux $\Psi \equiv \int_0^R 2\pi R' B_Z(Z, R', t)dR'$ and the out-of-plane magnetic field B_Y measured by the 2-D magnetic probe arrays during the quasi-steady period of a typical MRX jog discharge. The right column shows the quadrupolar B_Y structure moving in radially with temporal changes mainly due to the TF coil current ringing [16]. The radial motion of the current sheet is shown in the left column. The current sheet structure is well-maintained and moves in with the quadrupolar B_Y. The layer clearly has 2-D structures: J_Y varies along Z and the $B_Z = 0$ boundary indicated by red dashed lines is slightly kinked in the $R - Z$ plane, especially at $t = 340$ μs. However, the direction normal to the current sheet is generally along $\mathbf{e}_R$, the unit vector for R, as the curvature of the $B_Z = 0$ boundary remains small. The angle between the local vector normal to the boundary and $\mathbf{e}_R$ is less than 5 degrees. Furthermore, toroidal asymmetry monitored by an additional magnetic probe at $Y = -9$ cm is fairly negligible for this plasma. Therefore, the rotation matrix that transforms from (R, Y, Z) into (x, y, z) coordinates for this discharge should have diagonal terms close to unity and off-diagonal terms close to zero. In other words, $\hat{\mathbf{x}} \approx \mathbf{e}_R$, $\hat{\mathbf{y}} \approx \mathbf{e}_Y$, and $\hat{\mathbf{z}} \approx \mathbf{e}_Z$.

As shown in figure 5, data from four different measurement points ($Z = 0, 3, 6, 9$ cm; $R = 36.7$, $Y = 0$ for all) of the same discharge is used to test MVAB. At $Z = 0$, in the right vicinity of the X point, only the reconnecting magnetic field B_Z varies significantly as shown in figure 5-(c). In this case, variance of B_R is comparable to that of B_Y and the normal vector generated by MVAB becomes a mixture of $\mathbf{e}_R$ and $\mathbf{e}_Y$. The rotation matrix predicted by MVAB for this example is

$$\begin{pmatrix} x_1 \\ y_1 \\ z_1 \end{pmatrix} = \begin{pmatrix} 0.3576 & 0.9314 & 0.0682 \\ -0.9338 & 0.3560 & 0.0349 \\ 0.0082 & -0.0762 & 0.9971 \end{pmatrix} \begin{pmatrix} R \\ Y \\ Z \end{pmatrix}, \tag{7}$$

where the subscript 1 is added to avoid confusion and to emphasize these are just a 'suggested' coordinate system by MVAB at the given location. The normal vector is $0.3576\mathbf{e}_R + 0.9314\mathbf{e}_Y + 0.0682\mathbf{e}_Z$, which is even closer to $\mathbf{e}_Y$ than to the reference normal $\mathbf{e}_R$. Even though three eigenvalues of $\mathbf{M}$ are well-separated as shown in figure 5-(c'), the normal vector does not reflect the real magnetic geometry. The smallest and intermediate eigenvalues are often degenerate ($\lambda_1 \sim \lambda_2$) at $Z = 0$ in other discharges. However, MVAB predicts the direction of the reconnecting field well ($\hat{\mathbf{z}}_\mathbf{1} \simeq \mathbf{e}_Z$).

At $Z = 3$ cm, the quadrupolar out-of-plane field starts to play a role. While B_R remains small, B_Y changes moderately as shown in figure 5-(d). As a result, the three eigenvalues are well-separated and the unit vectors suggested by MVAB reflect the magnetic geometry. The coordinate system determined by MVAB is usually best at $Z = \pm 3$ cm for MRX jogging experiment data. The transformation matrix predicted by MVAB at this location is

$$\begin{pmatrix} x_2 \\ y_2 \\ z_2 \end{pmatrix} = \begin{pmatrix} 0.9976 & 0.0630 & 0.0297 \\ -0.0687 & 0.9601 & 0.2712 \\ -0.0115 & -0.2726 & 0.9621 \end{pmatrix} \begin{pmatrix} R \\ Y \\ Z \end{pmatrix}. \tag{8}$$

The normal vector from MVAB is very close to the reference normal. It is worth noting that $\hat{\mathbf{z}}_\mathbf{2}$ has been degraded as it picks up a sizeable $\mathbf{e}_Y$ component, which means the Hall field is considered as a part of the reconnecting field by MVAB. The predicted out-of-plane direction $\hat{\mathbf{y}}_\mathbf{2}$ also has a considerable $\mathbf{e}_Z$ component. Thus, as shown in figure 5-(d'), the quadrupolar component of B_{y2} is weakened after the coordinate transformation. This tendency is enhanced further downstream, so that the transformed out-of-plane magnetic field component B_y is significantly contaminated by the other two components as shown in figure 5-(e') and (f') and frequently loses its bipolar shape. This could be one of the reasons why a clear quadrupolar structure has been rarely identified in space [12].
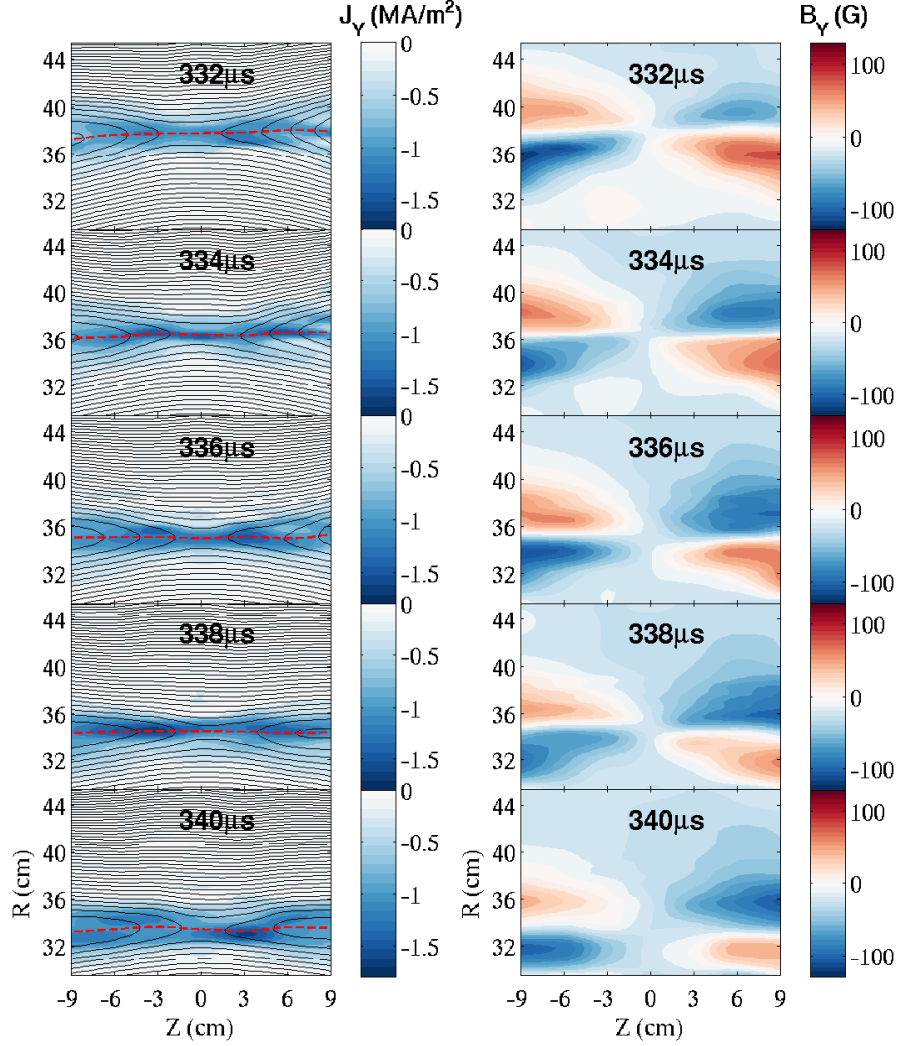
Figure 4: Data from 2-D magnetic probe arrays during the quasi-steady period of the MRX jog experiment discharge 114338 is shown. Colors in left panels demonstrate the profile of the current density J_Y, while the black lines mean contours of the poloidal flux Ψ. The red dashed lines indicate the location of $B_Z = 0$ boundary which agrees well with the current sheet location from the Harris fitting. Contour plots of the right panels show the time evolution of the out-of-plane magnetic field B_Y every 2 μs. Because of the time-varying TF current, the overall shape of the quadrupole structure undergoes temporal changes. The current sheet moves in radially together with the quadrupolar B_Y structure with a speed of ~ 6 km/s.
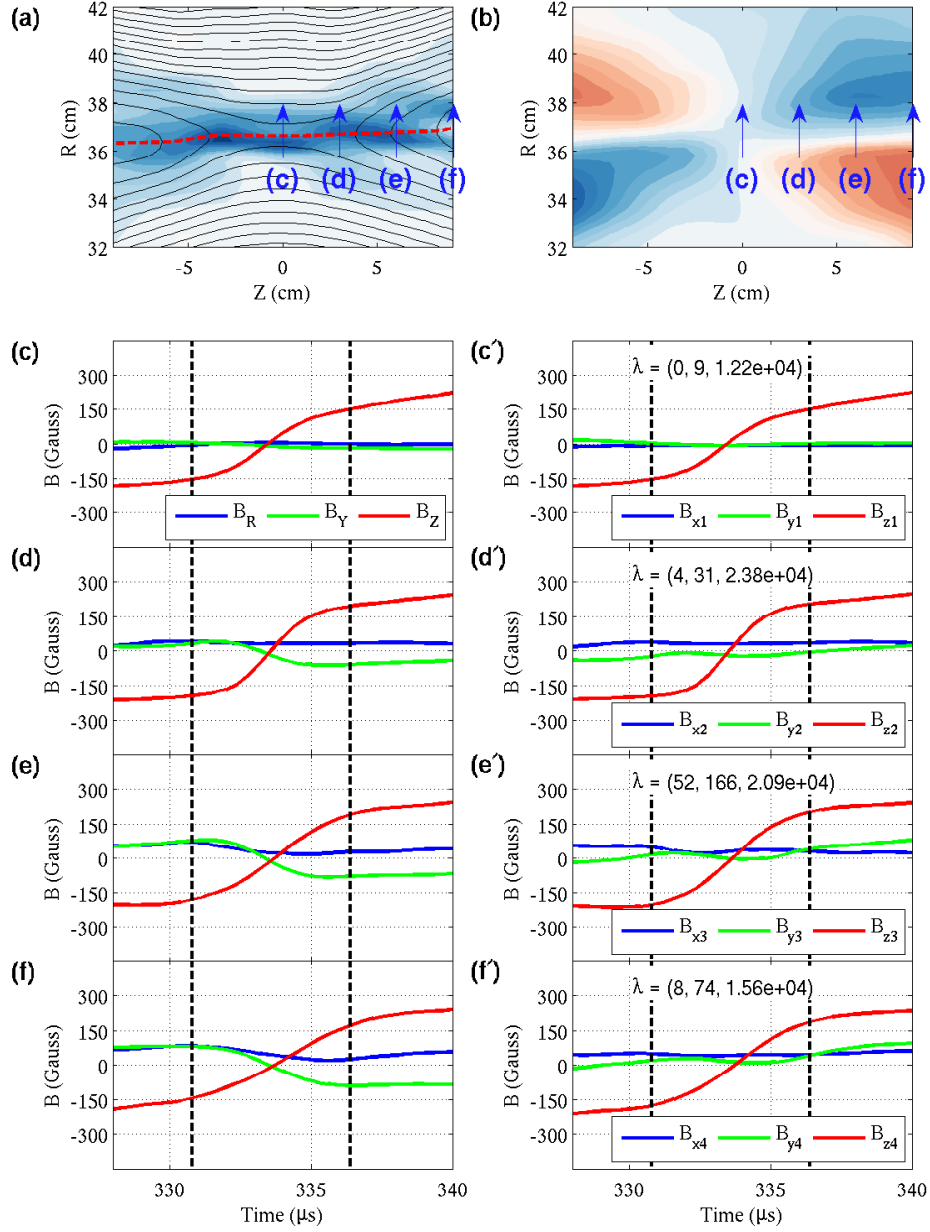
Figure 5: (a) 2-D profile of J_Y with contours of Ψ of the discharge 114338 at the time the current sheet is close to the sample measurement points. (b) That of B_T. Color scales are the same as in figure 4. The arrows indicate the data range used for MVAB. (c)(d)(e)(f) Magnetic field data at $(R, Z) = (36.7, 0)$, $(36.7, 3)$, $(36.7, 6)$, and $(36.7, 9)$ ($Y = 0$ for all) respectively around the time the current sheet passes. Data between dashed black lines is used for MVAB. (c′)(d′)(e′)(f′) Profiles in (x, y, z) coordinates suggested by MVAB. Three eigenvalues (λ) of the matrix $\mathbf{M}$ are shown inside of each panel. The out-of-plane magnetic field (B_Y) loses the bipolar shape after the coordinate transform by MVAB.

8

At $Z = 6$ cm, the variation in B_R becomes non-negligible because of the 2-D structure of the reconnection geometry. For most of cases, this leads a degenerate condition with $\lambda_1 \sim \lambda_2$, making $\hat{\mathbf{x}}_\mathbf{3}$ and $\hat{\mathbf{y}}_\mathbf{3}$ meaningless. The suggested transformation for this example is

$$\begin{pmatrix} x_3 \\ y_3 \\ z_3 \end{pmatrix} = \begin{pmatrix} 0.7990 & -0.5677 & -0.1984 \\ 0.5927 & 0.6876 & 0.4195 \\ -0.1017 & -0.4528 & 0.8858 \end{pmatrix} \begin{pmatrix} R \\ Y \\ Z \end{pmatrix}. \tag{9}$$

$\hat{\mathbf{z}}_\mathbf{3}$ is further deviated from $\mathbf{e}_Z$ and both $\hat{\mathbf{x}}_\mathbf{3}$ and $\hat{\mathbf{y}}_\mathbf{3}$ do not reflect the real magnetic geometry. Similar trends continue at $Z = 9$ cm where MVAB generates the following coordinate transformation:

$$\begin{pmatrix} x_4 \\ y_4 \\ z_4 \end{pmatrix} = \begin{pmatrix} 0.8542 & -0.5036 & -0.1291 \\ 0.4888 & 0.6935 & 0.5293 \\ -0.1770 & -0.5152 & 0.8386 \end{pmatrix} \begin{pmatrix} R \\ Y \\ Z \end{pmatrix}. \tag{10}$$

In this example, the suggested normal vector is again closer to $-\mathbf{e}_Y$ than to $\mathbf{e}_R$, which does not agree with the real magnetic geometry.

To confirm that the above disagreement of the normal vectors from MVAB with the measured magnetic geometry is not due to measurement noise, we perform error estimates following *Khrabrov and Sonnerup* [1998] [17] where errors associated with random noise in minimum/maximum variance analysis are analytically derived. In the reference, the angular uncertainty is given by

$$|\Delta\phi_{ij}| = |\Delta\phi_{ji}| = \sqrt{\frac{\lambda_1}{(M-1)} \frac{(\lambda_i + \lambda_j - \lambda_1)}{(\lambda_i - \lambda_j)^2}}, \ i \neq j, \tag{11}$$

where $|\Delta\phi_{ij}|$ is the angular uncertainty of eigenvector $\mathbf{u}_i$ in the direction of $\mathbf{u}_j$. The combined statistical error estimate for $\langle\mathbf{B}\rangle_n \equiv \langle\mathbf{B}\rangle \cdot \mathbf{u}_1$ is [15]

$$|\Delta\langle\mathbf{B}\rangle \cdot \mathbf{u}_1| = \sqrt{\frac{\lambda_1}{M-1} + (\Delta\phi_{12}\langle\mathbf{B}\rangle \cdot \mathbf{u}_2)^2 + (\Delta\phi_{13}\langle\mathbf{B}\rangle \cdot \mathbf{u}_3)^2}, \tag{12}$$

where the first term inside of the square root comes from the uncertainty in the average magnetic field associated with the variance λ_1.

Figure 6 shows the results of the error estimates with $M = 3$ to 41 for the same data used for MVAB in figure 5. Error bars in this figure are computed by the above equations. The estimated statistical errors in $\langle\mathbf{B}\rangle$ are generally small as shown in figure 6-(a), which is expected since the signal-to-noise ratio of MRX magnetic data is small. Figure 6-(b) and (c) show the angle between the normal vector from MVAB, $\mathbf{u}_1$, and the reference normal vector, $\mathbf{e}_R$, in the R-Y plane (ϕ_{RY}), and in the R-Z plane (ϕ_{RZ}) as a function of the nest size, M. When the normal vector from MVAB agrees with the measured global magnetic geometry, both ϕ_{RY} and ϕ_{RZ} are close to zero. Except at $Z = 3$ cm, ϕ_{RY} and ϕ_{RY} are not close to zero and statistical errors do not account for the difference. Therefore, the disagreement of the results from MVAB with the global magnetic geometry does not come from random noise.

MVAB is also tested in a discharge with a time-varying reconnection geometry. As shown in figure 7-(a), a clear O-point is developed and ejected downstream. This O-point is associated with very high local current density and is believed to have a 3-D structure [18], so we describe this feature as a "flux rope" to emphasize its 3-D nature even though it is not accompanied with a sizeable guide field. MVAB is conducted for data from the measurement point at $(R, Z) = (37.6, -6)$ (indicated by green diamond marks in figure 7-(a)) as the flux rope passes by. Due to the O-point structure, there is a bump in B_R around 334 μs as shown in figure 7-(b). B_R is supposed to have the minimum variance without the O-point. The transformation matrix produced by MVAB for this case is

$$\begin{pmatrix} x_5 \\ y_5 \\ z_5 \end{pmatrix} = \begin{pmatrix} 0.4401 & 0.8906 & -0.1150 \\ -0.8824 & 0.4052 & -0.2389 \\ -0.1662 & 0.2066 & 0.9642 \end{pmatrix} \begin{pmatrix} R \\ Y \\ Z \end{pmatrix}. \tag{13}$$
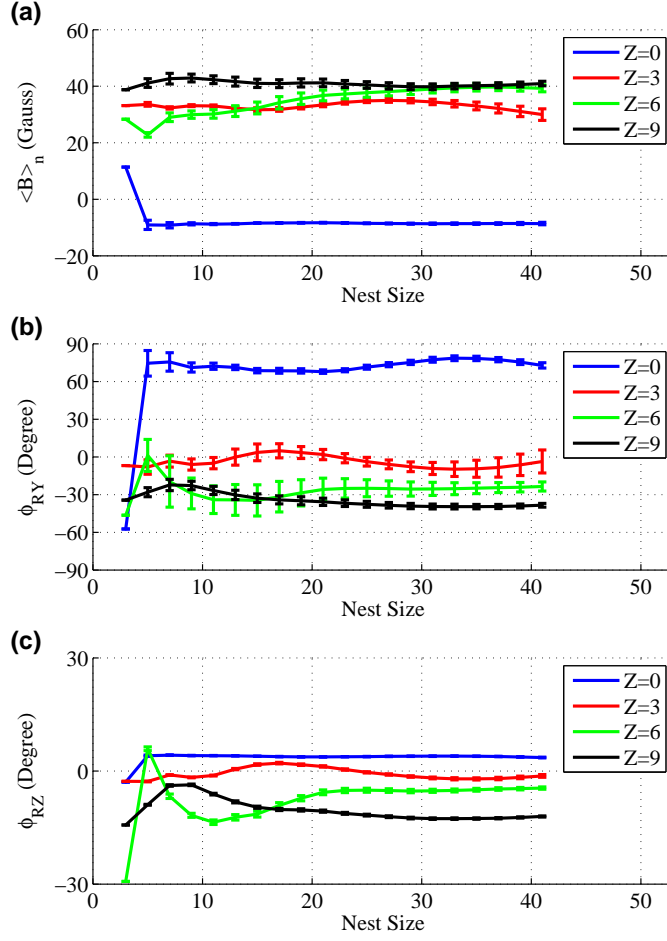
9

Figure 6: (a) Average magnetic field component along the suggested normal vector $\mathbf{u}_1$ from MVAB ($\langle\mathbf{B}\rangle_n \equiv \langle\mathbf{B}\rangle \cdot \hat{\mathbf{u}}_1$) as function of the nest size M. Error bars are computed by eq. (12). (b) ϕ_{RY} - Angle between $\mathbf{u}_1$ and the reference normal vector $\mathbf{e}_R$ in the R-Y plane - as function of M. Except at $Z = 3$, ϕ_{RY} is not close to zero for any value of M. (c) ϕ_{RZ} as function of M. ϕ_{RZ} is usually smaller than ϕ_{RY} since MVAB well-separates the direction of the reconnecting magnetic field from others.
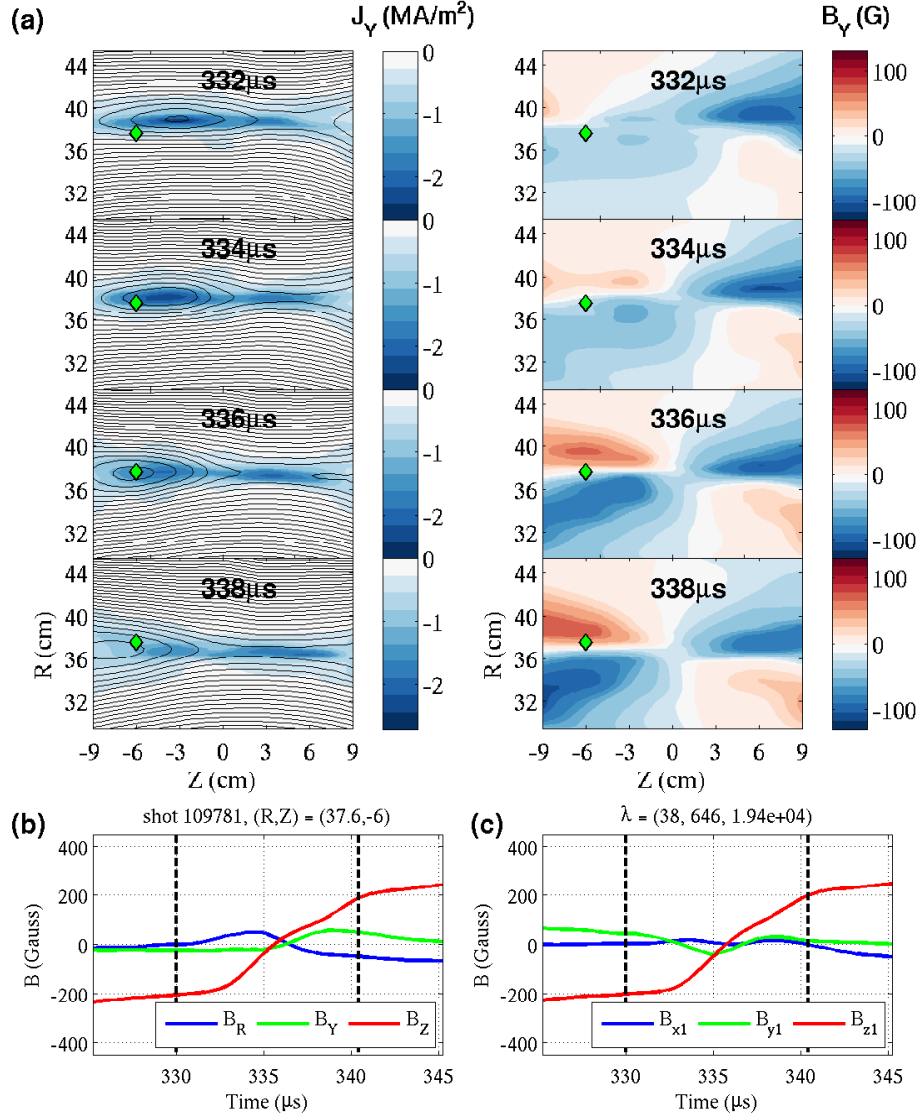
Figure 7: (a) Left panels: 2-D profiles of J_Y (color) with contours of Ψ of a discharge containing a flux rope. A clear O-point related to the high local current density is formed and ejected downstream. Right panels: 2-D profiles of B_Y. Initially, the left side of the quadrupolar structure is destroyed due to the development of the O-point structure ('flux rope'). As the flux rope is ejected downstream, the quadruopolar structure is recovered. The green diamond marks indicate the location of the sample measurement point for data shown in the panel (b). (b) Magnetic field data at a sample measurement point at $(R, Z) = (37.6, -6)$. The bump in the normal component B_R is caused by passing of the flux rope. (c) The same data after being transformed into the (x, y, z) coordinate system suggested by MVAB. Three eigenvalues are shown above the panel. Even though three eigenvalues are well-separated for this case, the (x, y, z) coordinate system constructed by MVAB is far from the real magnetic geometry.

Location	$\mathbf{u}_1$ (R,Y,Z)	$\mathbf{u}_3$ (R,Y,Z)	Eigenvalues
$\mathbf{r}_1$	(0.8871,0.4612,0.0182)	(-0.0288,0.0159,0.9995)	$3, 19, 2.07 \times 10^4$
$\mathbf{r}_2$	(0.9983,-0.0452,-0.0374)	(0.0501,0.3226,0.9452)	$1, 47, 1.37 \times 10^4$
$\mathbf{r}_3$	(0.9964,-0.0741,-0.0401)	(0.0149,-0.3134,0.9495)	$0.2, 23, 1.80 \times 10^4$
$\mathbf{r}_4$	(0.1002,-0.9942,-0.0388)	(-0.0056,0.0395,0.9992)	$0.2, 3, 1.35 \times 10^4$

Table 1: MVAB results for data from the same sample measurement points used for BCTA in figure 8. $\mathbf{u}_1$ is the suggested normal vector and $\mathbf{u}_3$ is the suggested direction of the reconnecting field.

Again, MVAB fails to predict a proper unit vector normal to the current sheet although three eigenvalues are well-separated as shown in figure 7-(c). However, it still produces a reasonable tangential vector as $\hat{\mathbf{z}}_5$ remains close to $\mathbf{e}_Z$.

These examples show that MVAB generally does not produce a proper normal vector even if the current sheet structure does not undergo significant time variations. However, MVAB is much better for determining the direction of the reconnecting magnetic field, the maximum-varying component, wich agrees with *Mozer and Retinó* [2007]. MVAB's prediction for $\hat{\mathbf{z}}$ is better for measurement points close to the X-point since variations of the other two components are smaller there.

5   Boundary-Crossing Time Analysis (BCTA)

If a 1-D boundary is crossed by multiple spacecraft, the following constraints [19] for the boundary normal direction $\hat{\mathbf{n}}$ and the relative velocity between the layer and the spacecraft $\mathbf{V}_{rel}$ can be found by assuming $\mathbf{V}_{rel}$ is a constant during the crossing:

$$(\mathbf{V}_{rel} \cdot \hat{\mathbf{n}})t_{\alpha\beta} = \mathbf{r}_{\alpha\beta} \cdot \hat{\mathbf{n}}, \tag{14}$$

where $\mathbf{r}_{\alpha\beta}$ is the separation vector between any pair of spacecraft and $t_{\alpha\beta}$ is the difference in time each spacecraft crosses the same boundary. For N spacecraft, one can find $N-1$ independent equations from the above constraint, so that the normal vector and relative velocity along the normal direction $V_n \equiv \mathbf{V}_{rel} \cdot \hat{\mathbf{n}}$ can be determined if there are four spacecraft and they are not in the same plane. This crossing time analysis has been applied to Cluster spacecraft data to identify a multiple X-line geometry [20, 21].

This technique is applied to MRX jogging experiments to see whether it predicts a proper $\hat{\mathbf{n}}$ and V_n. Data from the same discharge shown in figures 4, 5, and 6 is used. We choose three test measurement points $((R, Z) = (38.5, -3), (38.5, 3), \text{ and } (33.7, 0); Y = 0$ for all) that form a nearly equilateral triangle in the main measurement plane with leg length ~ 6 cm. One more measurement point is provided by an additional probe at $(R, Y, Z) = (36.5, -9, 0)$. These measurement points form a tetrahedron with the fourth point at $Y = -9$ cm approximately 10 cm from the others. The upstream density measured by a Langmuir probe for this discharge is about 4×10^{13} cm^{-3}, which leads to an ion skin depth of $\delta_i \equiv c/\omega_{pi} \approx 5.1$ cm for this deuterium plasma. Thus, the separation between measurement points is comparable to δ_i. Figure 8-(c) shows B_Z at each measurement point. The time when the $B_Z = 0$ boundary passes each measurement point is chosen to compute $t_{\alpha\beta}$ since $B_Z = 0$ is a good indicator of the current sheet location. The normal vector from eq.(14) is $\hat{\mathbf{n}} = 0.9985\mathbf{e}_R - 0.0426\mathbf{e}_Y - 0.0341\mathbf{e}_Z$ for this example, which is very close to the reference normal $\mathbf{e}_R$. The calculated V_n is -5.62 km/s. To see if this value is reasonable or not, the radial position of the $B_Z = 0$ boundary measured by the magnetic probe array at $Z = 0$ is plotted in figure 8-(d). The average radial velocity of the boundary while it passes all four measurement points is -5.56 km/s, which is in excellent agreement with the BCTA value.

To compare the results from BCTA with those from MVAB, we perform MVAB for data from the same measurement points. Table 1 summarizes MVAB results which have similar trends described in the previous section. First, the normal suggested vector $\mathbf{u}_1$ is close to the reference normal $\mathbf{e}_R$ at $Z = \pm 3$ ($\mathbf{r}_2$ and $\mathbf{r}_3$) but it becomes a mixture of $\mathbf{e}_Y$ and $\mathbf{e}_R$ at $Z = 0$ ($\mathbf{r}_1$ and $\mathbf{r}_4$). Second, MVAB determines the direction of the
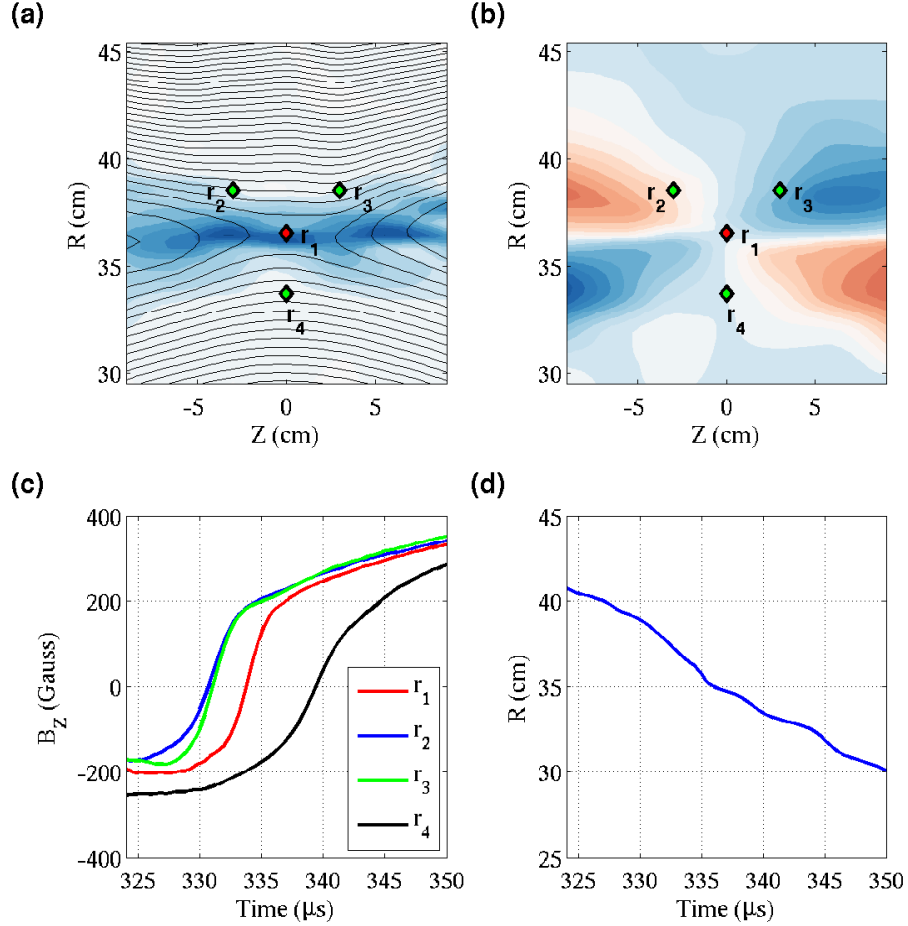
Figure 8: (a) Profile of J_Y with contours of Ψ of the discharge 114338 when the $B_Z = 0$ boundary is close to $\mathbf{r}_1$. (b) That of B_T. Four measurement points ($\mathbf{r}_1$, $\mathbf{r}_2$, $\mathbf{r}_3$, and $\mathbf{r}_4$) used for the boundary-crossing time analysis are shown in both panels. Those measurement points form a tetrahedron since $\mathbf{r}_1$, which is indicated by the red diamond mark, is actually 9 cm below of the main measurement plane. Color scales are the same as in figure 4. (c) B_Z profiles at 4 sample measurement points for $B_Z = 0$ boundary-crossing time analysis. The location of the measurement points in (R, Y, Z) coordinates is $\mathbf{r}_1 = (36.5, -9, 0)$, $\mathbf{r}_2 = (38.5, 0, -3)$, $\mathbf{r}_3 = (38.5, 0, 3)$, and $\mathbf{r}_4 = (33.7, 0, 0)$ respectively. (d) Radial location of the $B_Z = 0$ boundary measured by the magnetic probe array at $Z = 0$. The average radial velocity while the boundary passes through all four measurement points is -5.56 km/s.

reconnecting field component very well at $Z = 0$ but $\mathbf{u}_3$ is degraded at $Z = \pm 3$ as the Hall field is confused with the reconnecting field.

BCTA also predicts reasonable normal vectors for discharges that undergo significant temporal changes caused by 3-D structures. Figure 9-(a) shows the time evolution of J_Y with contours of Ψ and B_Y. At $t = 330\ \mu s$, the position of the main X-point is around $Z = 0$ based on the quadrupole B_Y structure. An O-point is formed around $Z = -3$ cm, generating another X-point probably around $Z = -11$ cm outside of the measurement window. It could be a secondary island in the 2-D picture [22], but here it is also a "flux rope" since there is a piece of evidence that proves it has 3-D structure. As shown in figure 9-(b), the $B_Z = 0$ boundary passes $\mathbf{r}_1 = (36.5, -9, 0)$ much earlier than $\mathbf{r}_5 = (36.4, 0, 0)$, indicating considerable toroidal asymmetry. This flux rope dynamically evolves changing the magnetic geometry significantly. As it moves toward the $+Z$ direction, the original X-point is pushed toward the same direction and the center of the quadruoplar B_Y structure is shifted to around $Z = -9$ cm, close to the second X-point, which means the most active X-point is now at $Z = -9$ cm. The same BCTA is done for this discharge to find $\hat{\mathbf{n}} = 0.9811\mathbf{e}_R - 0.1892\mathbf{e}_Y + 0.0392\mathbf{e}_Z$ and $V_n = -5.70$ km/s. $\hat{\mathbf{n}}$ has a sizeable $\mathbf{e}_Y$ component due to the toroidal asymmetry probably caused by kink-type instability along the out-of-plane current direction. The average radial velocity of the $B_Z = 0$ boundary from figure 9-(c) is -5.81 km/s. This velocity gives us -5.69 km/s of V_n which agrees well with the above value from BCTA.

6   Summary and Discussion

We have tested two major techniques for determination of the boundary normal direction in space with the use of data from the MRX jog experiment. Minimum variance analysis on the magnetic field when the measurement points passes through the current sheet generally does not predict a proper unit normal vector $\hat{\mathbf{n}}$, but it does duduce the direction of the reconnecting magnetic field well. The suggested $\hat{\mathbf{z}}$ is best in the vicinity of the X-point since the effect from the Hall field is smallest there. On the other hand, the normal vector suggested by $B_Z = 0$ boundary-crossing time analysis agrees well with the measured 3-D magnetic geometry. The velocity of the boundary $B_Z = 0$ along the normal vector is also in a good agreement with the radial speed of the current sheet measured by the 2-D magnetic probe arrays.

A fundamental reason MVAB sometimes fails to determine a proper normal vector is that the X-line magnetic geometry is at least 2-D. Let us explain this under the idealized 2-D X-line geometry shown in figure 10. The boundary of $\partial B_x/\partial x = 0$ coincides with the current sheet location at $x = 0$ and extends along the normal direction ($\hat{\mathbf{x}}$) only at $z = 0$. Because MVAB requires a finite number of samples of data around the boundary, at $z \neq 0$, MVAB naturally includes data from the region where $\partial B_x/\partial x = 0$ is not satisfied. Even at $Z = 0$, the variance of B_x is not guaranteed to be minimal since $\partial B_y/\partial x$ is also zero there. Actually, more than 50 percent of the tested cases for MRX jog experiment data at $Z = 0$ are degenerate ($\lambda_1 \sim \lambda_2$) since both B_R and B_Y do not change much.

The results in figure 6 support this idea. As shown in figure 6-(a), at $Z = 0$ in the vicinity of the X point, the length of the error bars becomes smaller with a large nest size M, which is expected by eqs. (11) and (12). On the other hand, error bars do not to change much at $Z \neq 0$. This is because the smallest eigenvalue λ_1 becomes larger as M increases, indicating the source of the variance is not from random noise but from something systematic: the magnetic geometry is not 1-D. With a larger data sample size, more data points lie in the region where $\partial B_x/\partial x \neq 0$, increasing the variance λ_1.

BCTA, on the other hand, is evaluated only during the moment that the boundary passes the measurement point. Therefore, as long as the boundary is close to a plane and $\mathbf{V}_{rel}$ is approximately constant over time, it generates a reasonable $\hat{\mathbf{n}}$ and V_n. As shown in figure 10, the $B_z = 0$ boundary is a straight line (a plane in 3-D) in spite of the 2-D X-line magnetic geometry. This is why crossing time analysis even works for discharges with flux ropes like figure 9. As shown in figure 9-(a), red dashed lines ($B_Z = 0$ boundaries) remain close to a straight line especially between $Z = \pm 3$ cm where crossing time analysis is employed.

For BCTA, the distance between measurement points (or spacecraft) is important. If the separation is too small, the normal vector only reflects the local geometry which can be different from the global geometry due to, for example, flux ropes and/or kinked current sheets. If it is too large, the basic assumption of the
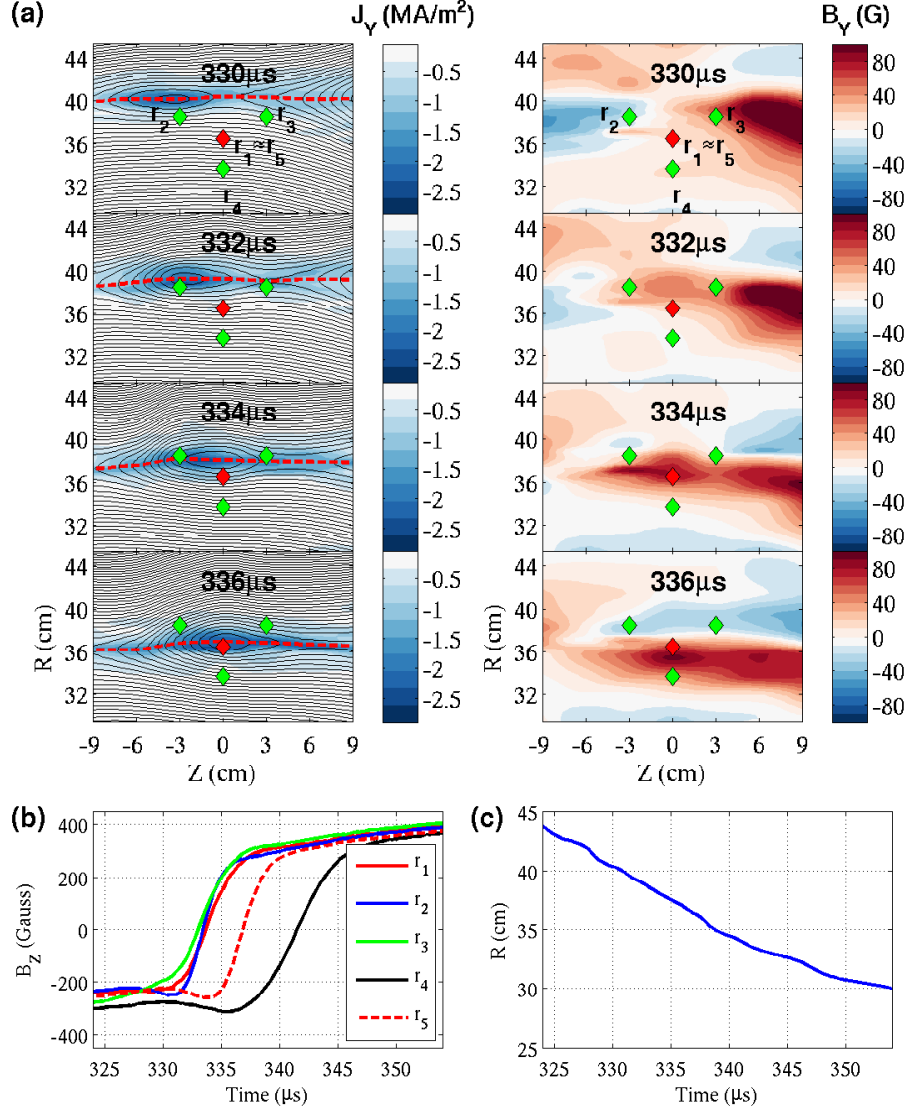
Figure 9: $B_Z = 0$ boundary-crossing time analysis (BCTA) for the discharge 114332 which has a 'flux rope' structure. (a) Left panels: 2-D profiles of J_Y (color) with contours of ψ. Red dashed lines stand for the $B_Z = 0$ boundary. Right panels: those of B_Y. A clear O-point is formed and moves to the $+Z$ direction changing magnetic geometry. The location of the measurement points are indicated by green and red diamonds. $\mathbf{r}_1$ and $\mathbf{r}_5$ has the same Z location and a similar R location, but $\mathbf{r}_1$ is located 9 cm below of the main measurement plane. (b) B_Z profiles at sample measurement points of $\mathbf{r}_1 = (36.5, -9, 0)$, $\mathbf{r}_2 = (38.5, 0, -3)$, $\mathbf{r}_3 = (38.5, 0, 3)$, $\mathbf{r}_4 = (33.7, 0, 0)$, and $\mathbf{r}_5 = (36.4, 0, 0)$ in (R, Y, Z). Although $\mathbf{r}_1$ and $\mathbf{r}_5$ have a similar radial position, the $B_Z = 0$ surface crosses $\mathbf{r}_1$ much earlier, which is a sign of toroidal asymmetry of this discharge. (c) Radial location of the $B_Z = 0$ boundary at $Z = 0$ and $Y = 0$. The average radial velocity of the boundary is -5.81 km/s.

15

$$B_z = 0,$$
$$\frac{\partial B_x}{\partial x} = 0.$$
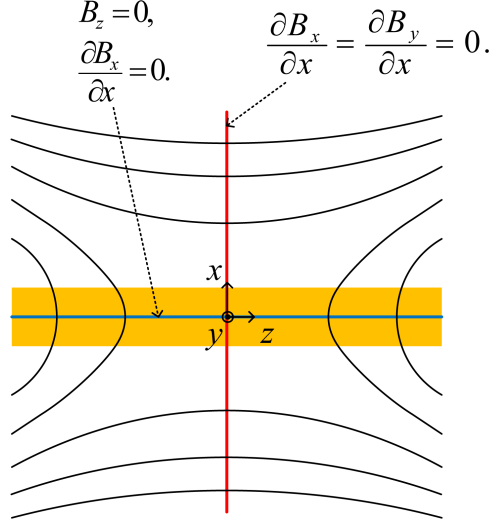$$\frac{\partial B_x}{\partial x} = \frac{\partial B_y}{\partial x} = 0.$$

Figure 10: Idealized X-line geometry. The orange box illustrates the current sheet. The blue line is the boundary of $B_z = 0$ where $\partial B_x/\partial x = 0$ is satisfied. The $\partial B_x/\partial x = 0$ extends along the x direction only at $z = 0$ (red line). $\partial B_y/\partial x = 0$ is also satisfied there.

boundary being a plane may not be satisfied. Moreover, the relative speed $\mathbf{V}_{rel}$ may not be considered to be a constant. For the MRX jog experiment, separation of $(1-2)\delta_i$ is proper because our system size is about $10\delta_i$ and the characteristic spatial scale of the kinked current sheet structure along toroidal direction is also expected to be comparable to the ion skin depth.

We suggest the following procedure for the determination of the magnetic geometry when four spacecraft passes through a current sheet layer. First, employ MVAB for all spacecraft data. Decide which spacecraft is closest to the X-point by either looking at other data such as the ion velocity or comparing λ_1 and λ_2 for each spacecraft. The one that has the smallest sum of λ_1 and λ_2 is mostly likely to be closest to the X-point. $\mathbf{u}_3$ from that spacecraft is a good indicator for $\hat{\mathbf{z}}$ and this is a temporary direction for the reconnecting magnetic field, $\hat{\mathbf{z}}'$. Find the time evolution of $B_{z'} = \mathbf{B} \cdot \hat{\mathbf{z}}'$ for each spacecraft. Then, estimate $\hat{\mathbf{n}} = \hat{\mathbf{x}}$ and V_n by crossing time analysis with the $B_{z'} = 0$ boundary. Since $\hat{\mathbf{n}}$ and $\hat{\mathbf{z}}'$ may not be orthogonal, decide $\hat{\mathbf{y}}$ first from $\hat{\mathbf{y}} = \hat{\mathbf{z}}' \times \hat{\mathbf{x}}$. Finally, $\hat{\mathbf{z}}$ is given by $\hat{\mathbf{z}} = \hat{\mathbf{x}} \times \hat{\mathbf{y}}$. The transformation matrix obtained by this procedure for data from the discharge 114338 is

$$\begin{pmatrix} x \\ y \\ z \end{pmatrix} = \begin{pmatrix} 0.9985 & -0.0426 & -0.0341 \\ 0.0420 & 0.9970 & -0.0146 \\ 0.0346 & 0.0132 & 0.9973 \end{pmatrix} \begin{pmatrix} R \\ Y \\ Z \end{pmatrix}, \tag{15}$$

which is very close to the desired identity matrix.

References

[1] M. Yamada, H. Ji, S. Hsu, T. Carter, R. Kulsrud, N. Bretz, F. Jobes, Y. Ono, and F. Perkins. Study of driven magnetic reconnection in a laboratory plasma. *Physics of Plasmas*, 4(5):1936–1944, 1997.

[2] M. Yamada, R. Kulsrud, and H. Ji. Magnetic reconnection. *Rev. Mod. Phys.*, 82:603–664, Mar 2010.

[3] M. Yamada. Progress in understanding magnetic reconnection in laboratory and space astrophysical plasmas. *Physics of Plasmas*, 14(5):058102, 2007.

[4] E. G. Zweibel and M. Yamada. Magnetic reconnection in astrophysical and laboratory plasmas. In R. Blandford, J. Kormendy, and E. VanDishoeck, editors, *Annual review of astronomy and astrophysics*, volume 47, pages 291–332. Annual Reviews, 2009.

[5] B. U. Ö. Sonnerup and L. J. Cahill. Magnetopause structure and attitude from explorer 12 observations. *J. Geophys. Res.*, 72:171, 1967.

[6] M. Øieroset, T.-D. Phan, M. Fujimoto, R. P. Lin, and R. P. Lepping. *In situ* detection of collisionless reconnection in the earth's magnetotail. *nature*, 412:414–417, 2001.

[7] B. U. Ö. Sonnerup, I. Papamastorakis, G. Paschmann, and H. Lühr. Magnetopause properties from ampte/irm observations of the convection electric field: Method development. *J. Geophys. Res.*, 92:12137–12159, 1987.

[8] G. Paschmann, B. U. Ö. Sonnerup, I. Papamastorakis, W. Baumjohann, N. Schopke, and H. Lühr. The magnetopause and boundary layer for small magnetic shear: Convection electric fields and reconnection. *Geophys. Res. Lett.*, 17:1829, 1990.

[9] T. Terasawa, H. Kawano, I. Shinohara, T. Mukai, Y. Saito, M. Hoshino, A. Nishida, S. Machida, T. Nagai, T. Yamamoto, and S. Kokubuns. On the determination of a moving mhd structure: Minimization of the residue of integrated faraday's equation. *J. Geomag. Geoelctr.*, 48:603–614, 1996.

[10] A. V. Khrabrov and B. U. Ö. Sonnerup. Orientation and motion of current layers: Minimization of the faraday residue. *Geophys. Res. Lett.*, 25:2373, 1998.

[11] C. T. Russell, M. M. Mellott, E. J. Smith, and J. H. King. Multiple spacecraft observations of interplanetary shocks: Four spacecraft determination of shock normals. *J. Geophys. Res.*, 88:4739 4748, 1983.

[12] F. S. Mozer and A. Retinò. Quantitative estimates of magnetic field reconnection properties from electric and magnetic field measurements. *J. Geophys. Res.*, 112:A10206, 2007.

[13] M. Yamada, H. P. Furth, W. Hsu, A. Janos, S. Jardin, M. Okabayashi, J. Sinnis, T. H. Stix, and K. Yamazaki. Quasistatic formation of the spheromak plasma configuration. *Phys. Rev. Lett.*, 46:188–191, Jan 1981.

[14] E. G. Harris. On a plasma sheath separating regions of oppositely directed magnetic field. *Nuovo Cimento*, 23:115, 1962.

[15] B. U. Ö. Sonnerup and M. Scheible. Minimum and maximum variance analysis. In G. Paschmann and P.W. Daly, editors, *Analysis Methods for Multi-Spacecraft Data*, pages 185–220. ISSI SR-001. EAS Publications Divisions, 1998.

[16] Y. Ren, M. Yamada, H. Ji, S. Dorfman, S. P. Gerhardt, and R. Kulsrud. Experimental study of the hall effect and electron diffusion region during magnetic reconnection in a laboratory plasma. *Phys. Plasmas*, 15:082113, 2008.

[17] A. V. Khrabrov and B. U. Ö. Sonnerup. Error estimates for minimum variance analysis. *J. Geophys. Res.*, 103:6641–6651, 1998.

[18] S. E. Dorfman. *Experimental study of 3-D, impulsive reconnection events in a laboratory plasma*. PhD thesis, Princeton University.

[19] S. J. Schwartz. Shock and discontinuity normals, mach numbers and related parameters. In G. Paschmann and P. W. Daly, editors, *Analysis Methods for Multi-Spacecraft Data*, pages 249–270. ISSI SR-001. EAS Publications Divisions, 1998.

[20] J. P. Eastwood, D. G. Sibeck, J. A. Slavin, M. L. Goldstein, B. Lavraud, M. Sitnov, S. Imber, A. Balogh, E. A. Lucek, and I. Dandouras. Observations of multiple x-line structure in the earths magnetotail current sheet: A cluster case study. *Geophys. Res. Lett.*, 32:L11105, 2005.

[21] J. P. Eastwood, T.-D. Phan, F. S. Mozer, M. A. Shay, M. Fujimoto, A. Retinò, M. Hesse, A. Balogh, E. A. Lucek, and I. Dandouras. Multi-point observations of the hall electromagnetic field and secondary island formation during magnetic reconnection. *J. Geophys. Res.*, 112:A06235, 2007.

[22] W. Daughton, J. Scudder, and H. Karimabadi. Fully kinetic simulations of undriven magnetic reconnection with open boundary conditions. *Physics of Plasmas*, 13(7):072101, 2006.

The Princeton Plasma Physics Laboratory is operated
by Princeton University under contract
with the U.S. Department of Energy.

Information Services
Princeton Plasma Physics Laboratory
P.O. Box 451
Princeton, NJ 08543

Phone: 609-243-2245
Fax: 609-243-2751
e-mail: pppl_info@pppl.gov
Internet Address: http://www.pppl.gov